# Sustainable Synthesis of Bacterial Cellulose Nanocrystals from Glucomannan-Based Bacterial Cellulose

**Tri Widjaja[1*], Siti Nurkhamidah[1], Hikmatun Ni'mah[1], Endarto Yudo Wardhono[2], Aisyah Alifatul Zahidah Rohmah[3], Anggi Tirta[1], Rossesari Nailah[1], and Citra Yulia Sari[1]**

[1]*Department of Chemical Engineering, Faculty of Industrial Technology and Systems Engineering, Institut Teknologi Sepuluh Nopember, Kampus ITS Sukolilo, Surabaya 60111, Indonesia*

[2]*Department of Chemical Engineering, Faculty of Engineering, Universitas Sultan Ageng Tirtayasa, Jl. Raya Jakarta Km. 4, Serang 42118, Indonesia*

[3]*Department of Chemical Engineering, Faculty of Engineering, Universitas Pembangunan Nasional "Veteran" Jawa Timur, Jl. Raya Rungkut Madya No. 1, Surabaya 60294, Indonesia*

**** Corresponding author:***

*email: trwi@chem-eng.its.ac.id*

*Received: August 23, 2024*
*Accepted: May 29, 2025*

**DOI:** 10.22146/ijc.99360

***Abstract:*** *Bacterial cellulose (BC), derived from glucose fermentation, is a renewable material known for its abundant availability, quick production, cost-effectiveness, and eco-friendly characteristics. This study focuses on converting BC into BC nanocrystals (BCNC) via fermentation, hydrolysis using acid solutions, and ultrasonication. Glucomannan flour with concentrations of 50, 60, and 90% was fermented using* Acetobacter xylinum *for 10 days at pH 5 to produce BC. The BC was then hydrolyzed with HCl solutions at 1, 2, 3, 4, and 5 M concentrations, followed by sonication. The 90% glucomannan flour yielded the highest BC amount (22.61 g). BCNC hydrolyzed with 1 M HCl exhibited the highest crystallinity (86%) and an elongated rod-like morphology. In contrast, hydrolysis with 4 and 5 M HCl caused carbonization, reducing crystallinity to below 30%. Particle size analysis showed the largest particle size for BCNC-2 (549.4 nm) and the smallest for BCNC-5 (207.2 nm). This research highlights the potential of glucomannan as a resource to produce BCNC for sustainable materials for various applications.*

***Keywords:*** *bacterial cellulose; bacterial cellulose nanocrystal; glucomannan; hydrolysis; sonication*

## ■ INTRODUCTION

Bacterial cellulose (BC) is a renewable and biodegradable material synthesized through the fermentation of glucose by specific bacterial strains. Unlike plant-derived cellulose, which requires extensive chemical processing to remove lignin and hemicellulose, BC is chemically pure and does not require additional purification [1-2]. Its environmentally friendly production uses energy and fewer chemicals while yielding cellulose with superior properties such as high tensile strength, excellent water-holding capacity, high crystallinity, a fine and pure fiber network, biocompatibility, and transparency [1]. These advantages have driven interest in BC as a sustainable alternative for a wide range of applications.

Previous studies have demonstrated the potential of agricultural waste substrates, such as coconut water, in BC production using *Acetobacter xylinum*, leading to products like nata de coco [3]. Coconut water, rich in nutrients such as sugars, proteins, and vitamins, supports bacterial growth while also addressing environmental concerns related to agro-industrial waste. Inspired by this approach, the current study explores porang tubers as an alternative substrate for BC production. In 2020, porang contributed significantly to Indonesia's export economy, with 14,568 tons or IDR 801.24 million in export value through porang chips [4], highlighting its availability and economic relevance.

Porang tubers contain approximately 64.28% glucomannan, a polysaccharide composed of glucose and mannose, which is highly valued for its functional properties in food and industrial applications. Glucomannan can be hydrolyzed into glucose, which serves as a carbon source for bacterial fermentation. The use of porang as a BC substrate introduces a cleaner and more sustainable method compared to traditional plant cellulose extraction, which often involves hazardous chemicals such as sodium hydroxide [5]. This strategy promotes environmental sustainability and local economic development through value-added utilization of abundant agricultural resources.

To further enhance the material properties of BC, it can be converted into BC nanocrystals (BCNC) via acid hydrolysis assisted by ultrasonication. This process removes amorphous cellulose regions, increases crystallinity, and reduces particle size, improving mechanical strength and dispersion [6-8]. Sonication also reduces the amount of acid required, making the process more environmentally friendly [9]. The resulting BCNC exhibits high potential for use in various high-value applications, including reinforcement in polymer matrices, food packaging, cosmetics, and biomedical materials [5,8-9], due to its superior crystallinity, modulus, and compatibility.

This study hypothesizes that BCNC derived from porang tubers through glucomannan fermentation and subsequent acid hydrolysis will exhibit enhanced material characteristics, including higher crystallinity and improved mechanical properties, compared to conventional sources. By optimizing the conversion of porang-based BC into BCNC, this research aims to provide a sustainable, high-performance nanomaterial that supports environmentally friendly industrial innovation and maximizes the economic value of a locally abundant resource.

## ■ EXPERIMENTAL SECTION

### Materials

Glucomannan flour with 50, 60, and 90% glucomannan content was obtained from PT Raja Porang (Madiun, Indonesia). *A. xylinum* bacteria were purchased commercially from a household custom fabrication facility in Sidoarjo, Indonesia. Distilled water was purchased from Sumber Ilmiah Persada (Surabaya, Indonesia). The HCl, NaOH, and $CH_3COOH$ were purchased from Sigma-Aldrich.

### Instrumentation

Preparing BCNC starts by sonicating the BC solution with a water bath sonicator (model Q55, Q-Sonica USA), which operates at a constant power of 100 W and a frequency of 40 Hz. A Nicolet iS5 spectrometer (Thermo Scientific, USA) was utilized to perform Fourier-transform infrared (FTIR) spectroscopy to identify the functional groups in BCNC. X-ray diffraction (XRD) analysis were conducted with a D8 Advance (Bruker, USA) instrument. The surface morphology of BCNC was studied by field emission scanning electron microscope (SEM) with a high-resolution JEOL-2100F SEM (Jeol, Japan), with an operating voltage of 30 kV.

### Procedure

#### *Preparation of BC*

The glucomannan flour varies in 50, 60, and 90% glucomannan content to obtain BC-1, BC-2, and BC-3 contents while the glucomannan fluor mass (2.5 g), distilled water (250 mL), and 0.5 M HCl (62.5 mL) were kept constant. The reason for varying the glucomannan content in the BC production is to determine the best raw material for producing the highest amount of BC up to 2.5 g of glucomannan flour was dissolved in distilled water at 1:100 (g/mL). The glucomannan in the solution was then hydrolyzed by adding 62.5 mL of 0.5 M HCl. Hydrolysis was performed with stirring at 120 °C for 20 min.

The hydrolyzed BC-1, BC-2, and BC-3 solutions were then cooled and neutralized in 0.5 M NaOH. The solution was centrifuged at 600 rpm at 5 °C for 10 min. The solution and solids from the centrifuge were separated, and the solution was removed. In total, 100 mL of this hydrolysis solution was dissolved in 400 mL of distilled water and sterilized in an autoclave. Furthermore, the sterilized solution was mixed with nutrients in the form of sugar (maximum 125 g) and

$(NH_4)_2SO_4$ (maximum 3 g). The solution mixture was then cooled to room temperature, after which the pH was measured, and $CH_3COOH$ was added until the pH of the solution reached 5. The solution was transferred into a previously sterilized container, and 10 mL of the *A. xylinum* bacteria was added. The 500 g solution containing bacteria was then fermented in an incubator for 10 days until BC formed. The BC formed during fermentation was washed and oven-dried at 70 °C for 48 h. The dried BC was ground and filtered into BC powder (100 mesh).

### *Preparation of BCNC*

The BC solution was prepared by dissolving 1 g of BC powder into 60 mL of HCl at various concentrations according to the predetermined values. The samples were named based on those variations, as shown in Table 1. The concentration range was chosen because it is expected to sufficiently demonstrate the effect of acid concentration in breaking down cellulose fibers without damaging their crystal structure, allowing control over the size and morphology of the resulting nanocrystals. This concentration is also considered safe and practical compared to higher concentration. Sonication was performed for 30 min at room temperature. After the sonication process, the BC solution was subjected to hydrolysis using HCl at 120 °C for 1 h to break down the cellulose fibers and form BCNC. The solution was then cooled and filtered. The filtered filtrate, BCNC, was then dried at 70 °C for 1 day.

### *Yield calculation for BC and BCNC*

The yield for BC was calculated by counting the mass of bacterial cellulose and comparing it with the initial mass of the solution that had fermented using Eq. (1).

$$\text{yield}(\%) = \frac{\text{mass of bacterial cellulose}}{\text{initial mass of solution}} \times 100\% \quad (1)$$

Meanwhile, the yield of BCNC is calculated using Eq. (2).

$$\text{yield}(\%) = \frac{\text{mass of BCNC}}{\text{initial mass of BC}} \times 100\% \quad (2)$$

### *BCNC characterization*

FTIR spectroscopy was performed to identify the functional groups present in BCNC. The analysis was conducted with a 4 $cm^{-1}$ resolution, from 650 to 4000 $cm^{-1}$, at a scanning speed of 20 mm/s. The crystallinity index (CrI) of BCNC was analyzed using XRD. The samples were scanned over a 2θ range from 10° to 40° at a speed of 1°/min using CuKa-filtered radiation. The crystallinity was calculated using the deconvolution method, where the diffraction profile was fitted with a Gaussian function to determine the contribution of each peak relative to the crystallographic plane and morphological background. CrI was calculated using Eq. (3).

$$\%\text{Crystallinity} = \frac{\text{Area of crystalline peaks}}{\text{Area of peaks (crystalline+Amorphous)}} \times 100\% \quad (3)$$

The morphology of the depolymerized cellulose was examined with SEM analysis. The samples were typically placed on a carbon-grid layer of copper: ImageJ (version 1.41h), and Origin 8 software analyzed particle size and diameter distribution. A particle size analyzer (PSA, Brookhaven, 90 plus, USA) is an instrument used to determine the distribution of particle sizes within a sample. Before analysis, BCNC was suspended in distilled water and treated with an ultrasonicator for 5 min.

**Table 1.** Sample code for BCNC production

| Sample code | Mass of BC (g) | HCl concentration (M) | Sonication time (min) | Sonication power (W) |
|---|---|---|---|---|
| BCNC-1 | 1 | - | - | - |
| BCNC-2 | | - | | |
| BCNC-3 | | 0.5 | | |
| BCNC-4 | | 1 | | |
| BCNC-5 | | 2 | 30 | 100 |
| BCNC-6 | | 3 | | |
| BCNC-7 | | 4 | | |
| BCNC-8 | | 5 | | |

## ■ RESULTS AND DISCUSSION

### Effect of Glucomannan Content on the Fermentation Yield of Bacterial Cellulose

BC derived from glucomannan flour with different glucomannan contents produced different yields and characteristics, as shown in Table 2. It can be seen that BC derived from 90% glucomannan flour was thicker than BC derived from 50 and 60% glucomannan flour. The total yield of bacterial cellulose in flour with a 90% concentration was significantly increased due to the high glucose content in the 90% glucomannan flour. The high glucose content is caused by the high level of glucomannan, which, when hydrolyzed with acid, breaks down into glucose. Glucose is a precursor in cellulose production and is a carbon source that influences bacterial growth. Therefore, the higher the glucose content in a substrate, the more it supports bacterial growth, forming more bacterial cellulose. This is why the 90% glucomannan flour has a very high nata de porang yield. The reactions that occurred in the fermentation process are shown in Eq. (4-7).

$$\text{Glucoce} + \text{ATP} \xrightarrow{\text{hexokinase}} \text{Glucose} - 6 - \text{phosphate} + \text{ADP} \quad (4)$$

$$\text{Glucoce} - 6 - \text{phosphate} \xrightarrow{\text{phosphoglucomutase}} \text{Glucose} - 1 - \text{phosphate} \quad (5)$$

$$\text{Glucose} - 1 - \text{phosphate} + \text{UTP} \xrightarrow{\text{glucose}-1-\text{phophate urydyltransferase}} \text{UDP} - \text{glucose} \quad (6)$$

$$\text{UDP} - \text{glucose} + (\text{glucose})_n \rightarrow \text{UDP} + (\text{glucose})_{n+1} \quad (7)$$

The bacteria used in the fermentation process are *A. xylinum*, as this bacterium can break down sugars to synthesize extracellular cellulose from glucose, maltose, and sucrose. Glucose, fructose, and glycerol have been identified as favourable carbon sources for cellulose biosynthesis. Under optimal conditions, cellulose was produced at a maximum rate of 36 g/d $m^2$, achieving a 100% yield from the added glucose [10] *A. xylinum* produces enzymes that polymerize sugars into thousands of fiber chains or cellulose through glycolysis [11]. Sucrose present in the glucomannan solution is broken down by *A. xylinum* into simpler sugars, namely glucose and fructose, with the help of the enzyme sucrase. The glucose formed from the hydrolysis of sucrose by sucrase is phosphorylated to form glucose-6-phosphate with the help of the hexokinase enzyme. Next, glucose-6-phosphate is converted into glucose-1-phosphate by the enzyme phosphoglucomutase through an isomerase reaction. Then, glucose-1-phosphate reacts with uridine triphosphate (UTP), assisted by the enzyme glucose-1-phosphate uridylyltransferase, forming uridine diphosphate glucose (UDP-glucose). Uridine diphosphate glucose (UDPG), which is a direct donor of glucose residues, with the help of the enzyme cellulose synthase, will form cellulose [12].

BC derived from 50 and 60% glucomannan flour was translucent (the color is not intense or transparent), whereas BC derived from 90% glucomannan flour was a milky white color, as shown in Fig. 1. Likewise, flour with both 50 and 60% glucomannan content had a low level of chewiness (can breakdown easily). In comparison, flour with 90% glucomannan content had high chewiness. BC produced from flour with 90, 50, and 60% glucomannan content had the most significant yield, at 45.22, 3.91, and 3.92% respectively. The yields derived from 50 and 60% glucomannan-containing flour are smaller than those of 90% glucomannan. Therefore, proceeding to the next stage of BCNC production was impossible.

**Table 2.** Bacterial cellulose fermentation with different glucomannan contents

| Glucomannan content (%) | 50 | 60 | 90 |
|---|---|---|---|
| Thickness (cm) | 0.1 | 0.2 | 1 |
| Color | Translucent | Translucent | Milky white |
| Chewiness level | Low | Low | High |
| Mass of BC (g) | 19.58 | 19.63 | 226.1 |
| Yield (%) | 3.91 | 3.92 | 45.22 |

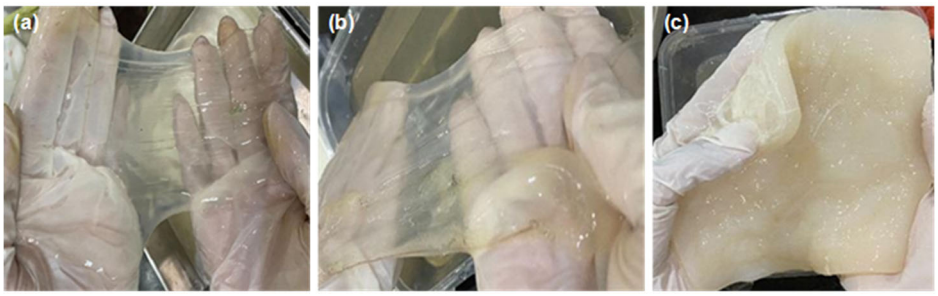


**Fig 1.** BC from (a) 50% glucomannan flour, (b) 60% glucomannan flour, and (c) 90% glucomannan flour

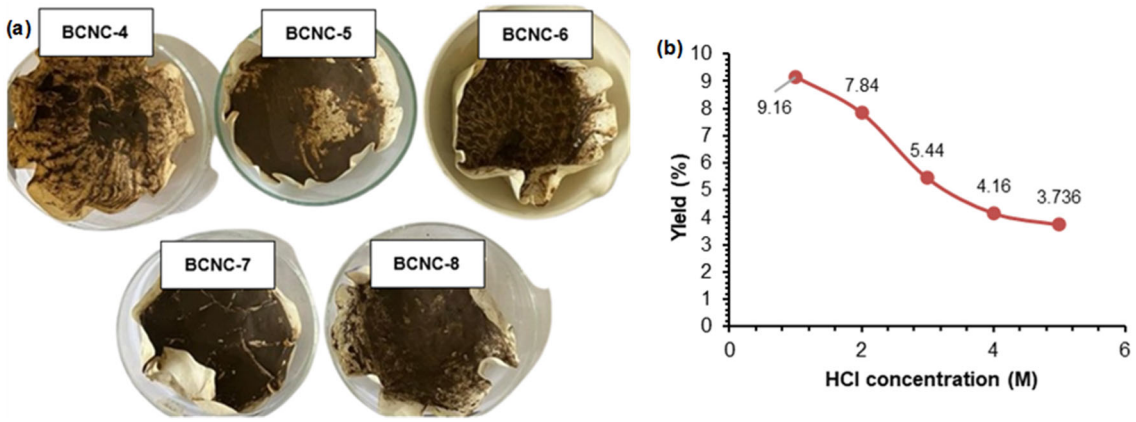


**Fig 2.** (a) BCNC photograph: BCNC-4 (HCl 1 M), BCNC-5 (HCl 2 M), BCNC-6 (HCl 3 M), BCNC-7 (HCl 4 M), and BCNC-8 (HCl 5 M); and (b) comparison of BCNC yield and HCl concentration

## Effect of Sonication Treatment and HCl Content on the Preparation of BCNC

The sonication effect of BC in a volatile liquid medium can depolymerize BC [1]. This result is demonstrated by the increase in CrI after sonication of BC. The volatile liquid medium plays a vital role in destroying the amorphous regions of BC and is beneficial for the accessibility of volatile liquid cavitation to isolate bacterial cellulose microcrystals (BCMC).

The effect of the HCl content on the hydrolysis of BCMC to form BCNC can be seen in greater detail in Fig. 2(a), which contains photographs of various BCNC. The BCNC with the lowest HCl concentration are lighter in color, whereas those with higher HCl concentrations are darker in color. This is because a higher HCl concentration damages the amorphous region, which promotes carbonization. Arserim-Uçar et al. [13] also reported that prolonged acid treatment weakens the crystalline structure, damaging the hydrogen chain and leading to carbonation.

Fig. 2(b) shows the relationship between the BCNC yield and the HCl concentration used in the hydrolysis process. The higher the HCl concentration, the lower the yield. The decrease in yield is caused by the higher concentration of HCl, which increasingly hydrolyzes the amorphous regions, while these regions have already degraded into water-soluble products [14]. The higher the acid concentration, the more amorphous areas of the cellulose are hydrolyzed into water-soluble monosaccharides, leaving fewer crystalline regions [15]. On the other hand, an excessively high acid concentration will lead to carbonization. This carbonization converts cellulose into carbon, resulting in a dark-colored product. The presence of carbonization indicates that both the amorphous and crystalline regions of the cellulose have begun to deteriorate. Therefore, the resulting yield will also drastically decrease.

## FTIR

FTIR analysis in this study determines the functional groups present in the raw material samples

(glucomannan flour), BC, and BCNC. The testing was conducted at the Water Technology and Industry Consultation Laboratory (TAKI), Department of Chemical Engineering, Institut Teknologi Sepuluh Nopember (ITS). Based on the FTIR analysis results, the spectra used were within the wavelength range of 600 to 4000 $cm^{-1}$, including the mid-IR spectrum. This spectrum range is divided into four regions: the single bond region (2500–4000 $cm^{-1}$), double bond region (1500–2000 $cm^{-1}$), triple bond region (2000–2500 $cm^{-1}$), and fingerprint region (600–1500 $cm^{-1}$). Table 3 shows the functional groups of BC and BCNC.

As we see in Fig 3, the FTIR spectra of bacterial cellulose and BCNC reveal characteristic vibration bands such as 3337 (O–H stretching), 1425 (asymmetric angle deformation of C–H bond), 1371 (symmetric angle deformation of C–H bond), 1425 (asymmetric angle deformation of C–H bond), and 110 $cm^{-1}$ (asymmetric stretching of glycosidic C–O–C bond). Several peaks indicate cellulose compounds. A broad absorption peak at 3337 $cm^{-1}$ indicates free O–H vibration induced by a cluster of hydroxyls in the cellulose molecules. The main functional groups composing glucomannan compounds are C–H at 2894, C–O–C at 1103, O–H at 3337 $cm^{-1}$, and the region from 760 to 860 $cm^{-1}$ indicates β-glycosidic and β-mannosidosis compounds, which are combinations of glucose and mannose structures. The absorption intensity at the wavenumber of 1617 in the glucomannan sample was higher than that in cellulose and bacteria because glucomannan has acetyl groups every 10–19 carbon units at positions C2, C3, and C6, where these acetyl groups have C=O bonds.

When comparing the FTIR spectra of bacterial cellulose and BCNC, both have very similar FTIR spectra because forming BCNC from bacterial cellulose only involves amorphous area erosion, and no compound

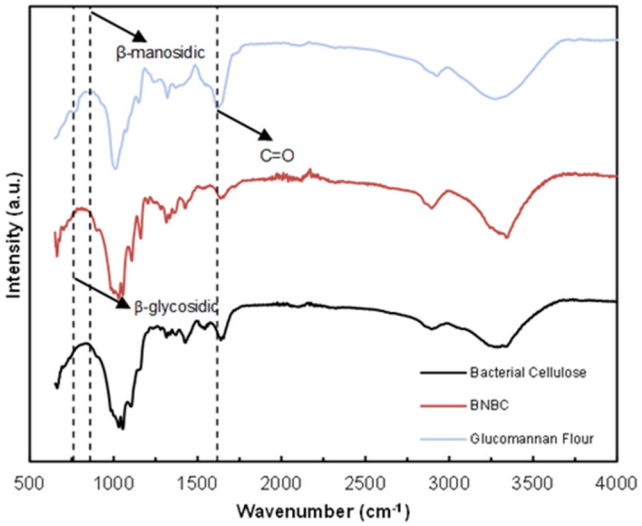


**Fig 3.** FTIR spectra of glucomannan flour (90%), BCNC-4, and bacterial cellulose

**Table 3.** FTIR spectra of glucomannan fluor, BC, and BCNC samples

| Wavenumber ($cm^{-1}$) | Glucomannan fluor | BC | BCNC |
|---|---|---|---|
| 760 | β-glycosidic compound | - | - |
| 860 | β-minoxidil compound | - | - |
| 900 | - | - | Asymmetric C–H (amorph) deformation |
| 1103 | Asymmetric C–O–C glycosidic bonds | Asymmetric C–O–C glycosidic bonds | Asymmetric C–O–C glycosidic bonds |
| 1371 | Deformation of symmetric C–H bond | Deformation of symmetric C–H bond | Deformation of symmetric C–H bond |
| 1425 | - | Deformation of asymmetric C–H bond | Deformation of asymmetric C–H bond |
| 1617 | C=O stretch | C=O stretch | C=O stretch |
| 2894 | Stretching of C–H bond from $CH_2$ | Stretching of C–H bond from $CH_2$ | Stretching of C–H bond from $CH_2$ |
| 3337 | Stretching O–H bond | Stretching O–H bond | Stretching O–H bond |

changes occur. The difference only occurs at the peak 900 $cm^{-1}$, where there is an asymmetric angle deformation of C–H in the amorphous region, which is only observed in BCNC that has undergone hydrolysis and sonication processes, causing damage to its amorphous area. These results agree with [16], which reported that CNC obtained through hydrolysis with $H_2SO_4$ and HCl has a chemical composition similar to that of bacterial cellulose [17].

## XRD

The XRD patterns of bacterial cellulose and BCNC, as shown in Fig. 4, show the highest peak at 2θ = 22.75° and other peaks at 2θ = 16.4° and 18.23°, indicating cellulose, which is consistent with [17]. According to [18], the XRD pattern of cellulose consists of a prominent peak at 2θ = 22.6° and a low diffraction intensity at 2θ = 16.4°. These angles appear in the bacterial cellulose and BCNC patterns. This indicates that hydrolysis with HCl and sonication can enhance and maintain the crystal position of bacterial cellulose to form BCNC. However, the higher intensity at the 22.6° peak in BCNC compared to bacterial cellulose suggests that sonication hydrolysis can increase the crystallinity of cellulose. The XRD patterns of the BCNC samples are shown in Fig. 5. BCNC with 1 M HCl exhibits peaks at 14.9°, 16.4°, and 22.6°, corresponding to the diffraction peaks of cellulose [18]. These peak characteristics are the same for BCNC containing 1, 2, and 3 M HCl.

However, at HCl concentrations exceeding 3 M, the cellulose transforms into an amorphous phase. This indicates that hydrolysis with HCl can maintain the crystallinity of cellulose at only specific concentrations and that under these conditions, cellulose undergoes degradation [19]. The crystallinity of BCNC was then calculated using Eq. (3). Furthermore, the peak at 22.6° decreased in intensity with an increase in HCl concentration. This indicates that excessively high HCl concentrations can cause cellulose degradation [19]. The

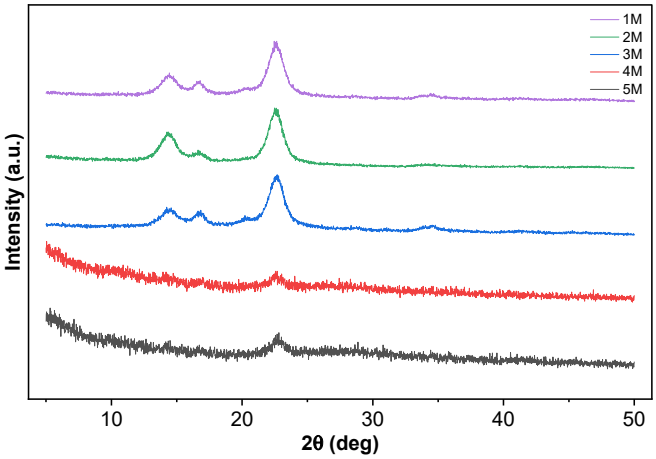


**Fig 5.** XRD patterns of BCNC prepared at various HCl concentrations

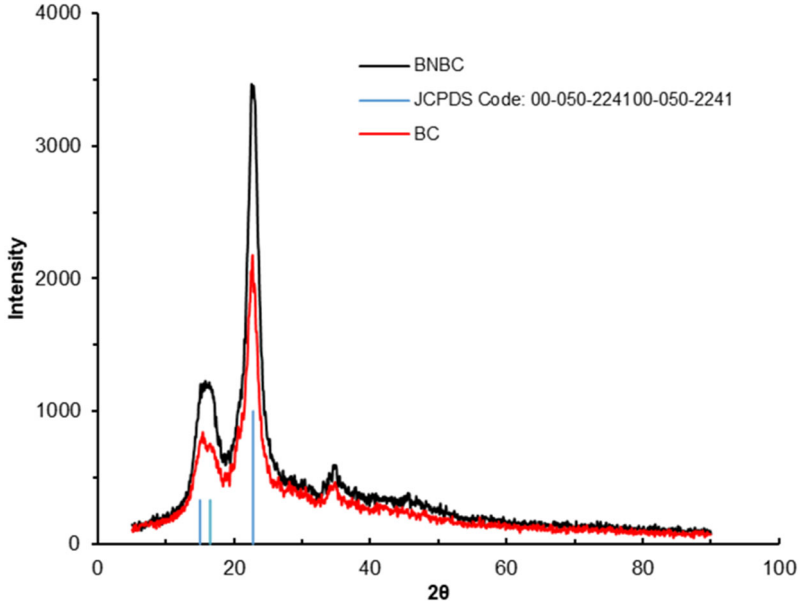


**Fig 4.** XRD spectra of BC and BCNC

Scherrer equation was used to estimate the crystallite size of BCNC. In the XRD test, besides examining two variables of BCNC that were treated with and without hydrolysis or sonication, we also tested samples of pure, untreated bacterial cellulose to observe the influence of the processes used on the crystallinity of BCNC, as shown in Tables 4 and 5.

The data in Table 4 shows that sonication treatment and hydrolysis by HCl affect the crystallinity of BCNC. BC without hydrolysis and sonication has crystallinity 48.592%, indicating that without hydrolysis, both amorphous and crystalline regions remain intact. At 0 M HCl and sonication for 30 min, the crystallinity of BCNC is 51.745%, indicating that sonication treatment can increase the CrI of bacterial cellulose. However, the crystallinity achieved is relatively low, which is still far from the commercial standard. This proves that sonication alone is insufficient to produce good quality BCNC that meet the standard. Hydrolysis treatment removes the amorphous regions of the cellulose polymer, resulting in highly crystalline single nanofibers. The sonication process helps to disperse the formed BCNC better and prevents agglomeration. Additionally, sonication aids hydrolysis in degrading the cellulose [20]. With the addition of 0.5 M HCl, there is a slight increase in crystallinity to 52.471%, indicating that some amorphous regions have been hydrolyzed. However, the acid concentration is still insufficient to enhance crystallinity significantly. The hydrolysis process can enhance crystallinity.

The data in Table 5 shows that HCl concentration significantly affects the crystallinity of BCNC. The 1 M HCl concentration yields the highest crystallinity of 86%, supporting the hypothesis that this is the optimal concentration for hydrolyzing the amorphous regions while preserving the crystalline regions, thereby forming high-quality BCNC. However, at 2 M HCl, the crystallinity decreases to 78.8%, showing that higher concentrations begin to damage the crystalline regions. Further decreases occur at 3, 4, and 5 M HCl concentrations, with crystallinity at 59, 28, and 26.7%, respectively, indicating that excessive hydrolysis damages both amorphous and crystalline regions, resulting in low-quality BCNC. This data reinforces that 1 M HCl is optimal for producing BCNC with high crystallinity.

Sonication treatment and hydrolysis can increase the CrI of bacterial cellulose. However, the crystallinity obtained was at a low index (around 50%), far below the commercial standard. This proves that more than sonication is needed to form good-quality BCNCs and meet commercial standards. Although the yield was high and capable of increasing the crystallinity of bacterial cellulose, its quality did not meet the commercial standard in terms of the CrI (< 70%). Therefore, acid hydrolysis is required to form BCNC that meets the standards. Hydrolysis removes the amorphous regions of the cellulose polymer, resulting in highly crystalline single nanofibers. The sonication process helps disperse the formed BCNC more evenly and eliminates clustering in BCNC. Additionally, sonication aids in hydrolysis to degrade cellulose [20].

## PSA

The particle size distributions and zeta potentials of all BCNC suspensions were measured, as shown in Fig. 6. BCNC-2 had the largest particle diameters of 549.4 and 207.2 nm, followed by BCNC-5 (408.4 nm),

**Table 5.** BCNC crystallinity with various HCl concentrations (M)

| Sample code | Crystallinity (%) |
|---|---|
| BCNC-4 (1 M HCl) | 86.0 |
| BCNC-5 (2 M HCl) | 78.8 |
| BCNC-6 (3 M HCl) | 59.0 |
| BCNC-7 (4 M HCl) | 28.0 |
| BCNC-8 (5 M HCl) | 26.7 |

**Table 4.** Comparison of the crystallinity of BC and BCNC with sonication and acid hydrolysis treatment

| Sample | Power (W) | Time (min) | HCl concentration(M) | Crystallinity (%) |
|---|---|---|---|---|
| BC | - | - | - | 48.592 |
| BCNC-1 | 100 | 30 | 0 | 51.745 |
| BCNC-2 | 100 | 30 | 0.5 | 52.471 |

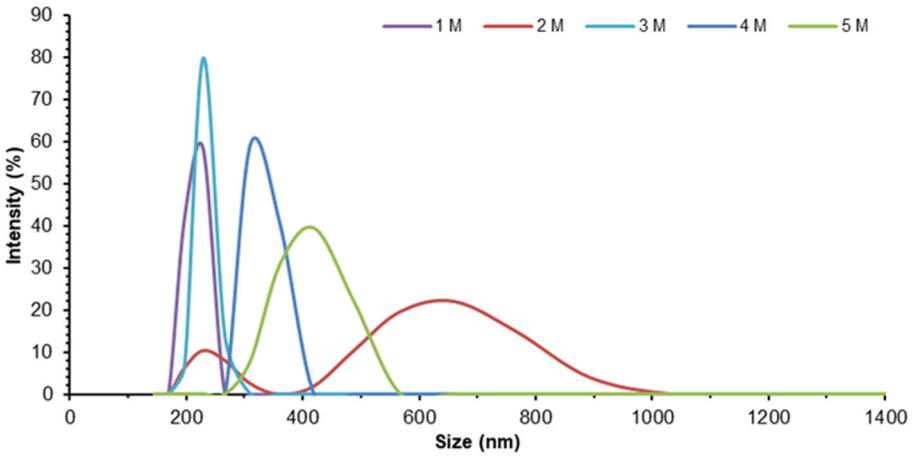


**Fig 6.** PSA results for BCNC

BCNC-4 (331.3 nm), BCNC-3 (216.3 nm), and BCNC-1 (232.5 nm). According to literature review [21], cellulose nanocrystals (CNC) have a length ranging from 100 to 1000 nm. Therefore, the PSA data shows that the synthesized BCNC falls within the nano-size category. The particle diameter generally decreased as the HCl concentration increased from 1 to 3 M. However, it increased at HCl concentrations above 3 M (4 and 5 M). The higher the acid concentration, the smaller the diameter of the BCNC particles. However, at 4 and 5 M, where the conditions are too acidic, the diameter increases and becomes increasingly irregular. This is because, under excessively acidic conditions, the structures of BCNC that have formed crystals can be restored to an amorphous form [22-23].

The results demonstrate a clear trend in the relationship between HCl concentration and particle size, highlighting the importance of controlling acid concentration during the preparation of BCNC. At lower concentrations (1–3 M), the acid effectively hydrolyzes the cellulose, leading to smaller, more uniform nanoparticles. However, at higher concentrations (4–5 M), the excessive acidity disrupts the crystalline structure, causing the particles to revert to a larger, amorphous state. This phenomenon underscores the delicate balance required in acid hydrolysis to achieve the desired nanoparticle characteristics. Additionally, the irregular particle sizes observed at higher acid concentrations could have implications for applying BCNC in fields where uniform particle size and stability are critical. Therefore, optimizing the acid concentration is essential for achieving the ideal particle size and maintaining the structural integrity and functional properties of BCNC. These findings are consistent with the SEM analysis, which also indicated variations in particle morphology corresponding to the changes in HCl concentration.

## SEM

The morphologies of BC and BCNC were analyzed using SEM at a magnification of 300. The results of the SEM analysis of BC, optimal-condition BCNC (HCl 1 M), and carbonized BCNC (HCl 5 M) are presented. BCNC is cellulose with an elongated rod-shaped structure, indicating only cellulose crystalline domains [23]. Fig. 7(a) shows the morphology of untreated BC, which exhibits a compact aggregate structure of bacterial cellulose without forming bacterial cellulose nanocrystals. In contrast, Fig. 7(b) illustrates the morphology of BCNC subjected to hydrolysis-sonication treatment with HCl 1 M, revealing that an elongated rod-shaped morphology characterizes the degradation of BC into BCNC. Subsequently, Fig. 7(c) displays the morphology of BCNC treated with hydrolysis-sonication using HCl 5 M, indicating the disrupted structure of BCNC with no longer an elongated rod-shaped morphology. This likely occurred because, at a concentration of 5 M, BCNC was carbonized, as supported by the XRD and crystallinity results. The data indicates that the crystallinity of BCNC

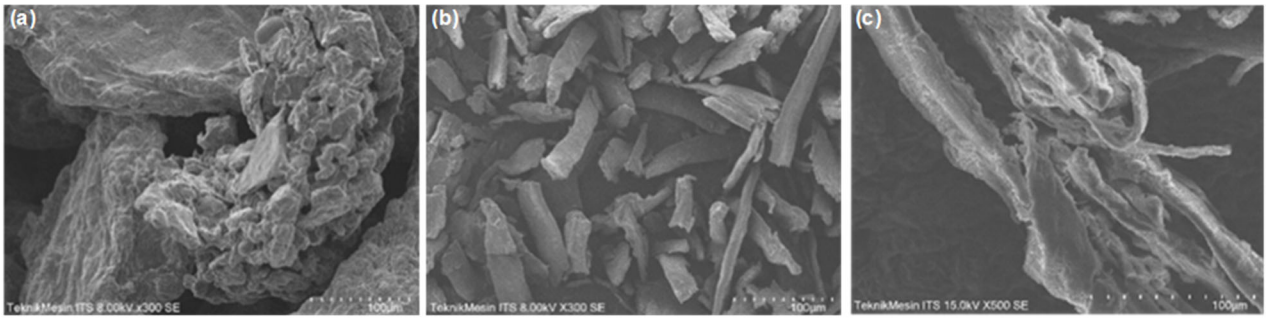


**Fig 7.** SEM images of (a) BC, (b) BCNC produced by HCl 1, and (c) 5 M

treated with HCl 5 M is very low at 26.7%, and the peak at 2θ = 22.5° is very low, indicating cellulose structural damage due to carbonization.

Visually, the diameter of the produced BCNC was large compared to the CNC sizes reported in the literature. According to the SEM results, the size of BCNC in Fig. 7(b) ranges from 4–6 μm in width and 40–50 μm in length. This may be due to the less optimal sonication power due to equipment limitations, which can only perform sonication up to 250 W. In another study [24], CNCs were successfully synthesized from recycled pulp using a sonication power of 1000 W. In addition to being generally larger than typical BCNC, these results also contradict the results shown in the PSA test. The SEM test is not accurate enough to detect cellulose particles at the nanoscale. In the PSA test, the BCNC sample was tested in suspension form, while in the SEM test, the BCNC sample was tested in solid form, which is still prone to aggregation. This phenomenon demonstrates that the behavior of cellulose crystals in solutions is significantly different from their behavior in the solid state. The surface charge of CNCs allows them to be highly dispersed in solution, enabling precise observation of nanoscale particles [23].

Hydrothermal treatment under subcritical or supercritical conditions efficiently decomposes biomass, waste polymers, and other halogen-containing compounds [19]. Subcritical or supercritical water has very different properties from those of environmental conditions. As a reaction medium, certain biopolymer materials such as cellulose, lignin, proteins, and starch can react in a short time at high temperatures with high system conversion [25]. Hydrothermal hydrolysis processes, therefore, tend to require lower acid concentrations but considerably more energy than ordinary hydrolysis processes, which require higher acid concentrations but little energy and are simple processes.

## ■ CONCLUSION

This study examines the manufacturing of BCNC using environmentally friendly methods. Higher glucomannan levels resulted in higher yields of glucomannan flour hydrolysis. BCNC was subjected to hydrolysis treatment using 1 M HCl, and sonication yielded the highest crystallinity (86%). Furthermore, these BCNC exhibited a well-defined morphology characterized by elongated rod-like structures, as evidenced by SEM analysis. Conversely, BCNC treated with hydrolysis using 4 and 5 M HCl concentrations underwent carbonization, resulting in crystallinity below 30% and SEM analysis showing a lack of morphological resemblance to typical BCNC. PSA revealed the largest particle diameter was for BCNC-2 (549.4 nm), followed by BCNC-4 (408.4 nm), BCNC-3 (331.3 nm), BCNC-1 (232.5 nm), and BCNC-5 (207.2 nm). This research highlights the potential of glucomannan as a resource to produce BCNC for sustainable materials of various applications.

## ■ ACKNOWLEDGMENTS

The authors would like to express their gratitude to the Directorate of Research Funding and Innovation, National Research and Innovation Agency in RIIM research, for their financial support, which was provided through grant numbers 6/IV/KS/05/2023 and 1179/PKS/ITS/2023. Additionally, the authors would like to thank LPDP (*Lembaga Pengelola Dana Pendidikan*) for their financial support in this research.

## ■ CONFLICT OF INTEREST

The authors declare no conflict of interest.

## ■ AUTHOR CONTRIBUTIONS

Siti Nurkhamidah conceptualized the study, designed the methodology, and led the manuscript writing. Hikmatun Ni'mah, Endarto Yudo Wardhono, and Aisyah Alifatul Zahidah Rohmah contributed to data collection and experimental analysis. Anggi Tirta and Rossesari Nailah assisted in data interpretation and visualization. Citra Yulia Sari supported the literature review and manuscript editing. Tri Widjaja supervised the research, provided critical revisions, and served as the corresponding author.

## ■ REFERENCES

[1] Wardhono, E.Y., Kanani, N., and Alfirano, A., 2020, A simple process of isolation microcrystalline cellulose using ultrasonic irradiation, *J. Dispersion Sci. Technol.*, 41 (8), 1217–1226.

[2] Ul-Islam, M., Khan, S., Ullah, M.W., and Park, J.K., 2019, Comparative study of plant and bacterial cellulose pellicles regenerated from dissolved states, *Int. J. Biol. Macromol.*, 137, 247–252.

[3] Wang, T., and Zhao, Y., 2021, Optimization of bleaching process for cellulose extraction from apple and kale pomace and evaluation of their potentials as film forming materials, *Carbohydr. Polym.*, 253, 117225.

[4] Sholichah, E., Purwono, B., Murdiati, A., Syoufian, A., and Sarifudin, A., 2023, Extraction of glucomannan from porang (*Amorphophallus muelleri* Blume) with freeze-thaw cycles pre-treatment, *Food Sci. Technol.*, 43, e1423.

[5] Naomi, R., Bt Hj Idrus, R., and Fauzi, M.B., 2020, Plant- vs. bacterial-derived cellulose for wound healing: A review, *Int. J. Environ. Res. Public Health*, 17 (18), 6803.

[6] Poddar, M.K., and Dikshit, P.K., 2021, Recent development in bacterial cellulose production and synthesis of cellulose based conductive polymer nanocomposites, *Nano Sel.*, 2 (9), 1605–1628.

[7] Abraham, E., Kam, D., Nevo, Y., Slattegard, R., Rivkin, A., Lapidot, S., and Shoseyov, O., 2016, Highly modified cellulose nanocrystals and formation of epoxy-nanocrystalline cellulose (CNC) nanocomposites, *ACS Appl. Mater. Interfaces*, 8 (41), 28086–28095.

[8] Özdemir, B., and Nofar, M., 2021, Effect of solvent type on the dispersion quality of spray-and freeze-dried CNCs in PLA through rheological analysis, *Carbohydr. Polym.*, 268, 118243.

[9] Wardhono, E.Y., Wahyudi, H., Agustina, S., Oudet, F., Pinem, M.P., Clausse, D., Saleh, K., and Guénin, E., 2018, Ultrasonic irradiation coupled with microwave treatment for eco-friendly process of isolating bacterial cellulose nanocrystals, *Nanomaterials*, 8 (10), 859.

[10] Masaoka, S., Ohe, T., and Sakota, N., 1993, Production of cellulose from glucose by *Acetobacter xylinum*, *J. Ferment. Bioeng.*, 75 (1), 18–22.

[11] Lahiri, D., Nag, M., Dutta, B., Dey, A., Sarkar, T., Pati, S., Edinur, H.A., Abdul Kari, Z., Mohd Noor, N.H., and Ray, R.R., 2021, Bacterial cellulose: Production, characterization, and application as antimicrobial agent, *Int. J. Mol. Sci.*, 22 (23), 12984.

[12] Barnes, W.J., and Anderson, C.T., 2018, Cytosolic invertases contribute to cellulose biosynthesis and influence carbon partitioning in seedlings of *Arabidopsis thaliana*, *Plant J.*, 94 (6), 956–974.

[13] Arserim-Uçar, D.K., Korel, F., Liu, L., and Yam, K.L., 2021, Characterization of bacterial cellulose nanocrystals: Effect of acid treatments and neutralization, *Food Chem.*, 336, 127597.

[14] Evcil, T., Simsir, H., Ucar, S., Tekin, K., and Karagoz, S., 2020, Hydrothermal carbonization of lignocellulosic biomass and effects of combined Lewis and Brønsted acid catalysts, *Fuel*, 279, 118458.

[15] Zhou, L., Huang, Y., He, X., Qin, Y., Dai, L., Ji, N., Xiong, L., and Sun, Q., 2022, Efficient preparation of cellulose nanocrystals with a high yield through simultaneous acidolysis with a heat–moisture treatment, *Food Chem.*, 391, 133285.

[16] Vasconcelos, N.F., Feitosa, J.P.A., da Gama, F.M.P., Morais, J.P.S., Andrade, F.K., de Souza Filho, M.S.M., and Rosa, M.F., 2017, Bacterial cellulose nanocrystals produced under different hydrolysis conditions: Properties and morphological features, *Carbohydr. Polym.*, 155, 425–431.

[17] Andritsou, V., de Melo, E.M.., Tsouko, E., Ladakis, D., Maragkoudaki, S., Koutinas, A.A., and Matharu, A.S., 2018, Synthesis and characterization of bacterial cellulose from citrus-based sustainable resources, *ACS Omega*, 3 (8), 10365–10373.

[18] De Filippis, P., de Caprariis, B., Scarsella, M., and Verdone, N., 2014, The hydrothermal decomposition of biomass and waste to produce bio-oil, *WIT Trans. Ecol. Environ.*, 180, 445–451.

[19] Wang, Y., Pääkkönen, T., Miikki, K., Maina, N.H., Nieminen, K., Zitting, A., Penttilä, P., Tao, H., and Kontturi, E., 2023, Degradation of cellulose polymorphs into glucose by HCl gas with simultaneous suppression of oxidative discoloration, *Carbohydr. Polym.*, 302, 1203880.

[20] Shojaeiarani, J., Bajwa, D., and Holt, G., 2020, Sonication amplitude and processing time influence the cellulose nanocrystals morphology and dispersion, *Nanocomposites*, 6 (1), 41–46.

[21] Jonoobi, M., Oladi, R., Davoudpour, Y., Oksman, K., Dufresne, A., Hamzeh, Y., and Davoodi, R., 2015, Different preparation methods and properties of nanostructured cellulose from various natural resources and residues: A review, *Cellulose*, 22 (2), 935–969.

[22] Shaheen, T.I., and Emam, H.E., 2018, Sono-chemical synthesis of cellulose nanocrystals from wood sawdust using acid hydrolysis, *Int. J. Biol. Macromol.*, 107, 1599–1606.

[23] Li, W., Yue, J., and Liu, S., 2012, Preparation of nanocrystalline cellulose via ultrasound and its reinforcement capability for poly(vinyl alcohol) composites, *Ultrason. Sonochem.*, 19 (3), 479–485.

[24] Filson, P.B., and Dawson-Andoh, B.E., 2009, Sono-chemical preparation of cellulose nanocrystals from lignocellulose derived materials, *Bioresour. Technol.*, 100 (7), 2259–2264.

[25] Kraśniewska, K., Galus, S., and Gniewosz, M., 2020, Biopolymers-based materials containing silver nanoparticles as active packaging for food applications–A review, *Int. J. Mol. Sci.*, 21 (3), 698.